Mechanically switchable wetting on wrinkled elastomers with dual-scale roughness

Pei-Chun Lin[ab] and Shu Yang*[a]

Received 14th August 2008, Accepted 24th November 2008
First published as an Advance Article on the web 22nd January 2009
DOI: 10.1039/b814145b

We report the fabrication of a new superhydrophobic surface with dual-scale roughness by coating silica nanoparticles on a poly(dimethylsiloxane) (PDMS) elastomer bilayer film with micro-scaled ripples. The wetting behavior of the surface can be reversibly tuned by applying a mechanical strain, which induces the change in micro-scale roughness determined by the ripples. The dual-scale roughness promotes the wetting transition of the final dual-structure surface from Wenzel region into the Cassie region, thus, reducing the sliding angle at least three times in comparison to that from the surfaces with single-scale roughness (either from the nanoparticle film or the wrinkled PDMS film). In addition, three-times and fast-response tunability of the sliding angle by applying mechanical strain on this dual-roughness surface is demonstrated.

Introduction

The ability to dynamically tune the surface properties (such as wetting, adhesion and friction) of a material in a controlled fashion is highly desirable for many emerging applications, including microfluidics, micro- and nanofabrication of complex structures, robotics, and cell attachment. Generally, wetting behavior is strongly dependent on both surface chemistry (*i.e.* surface energy) and surface topography (*i.e.* physical roughness). Many groups have attempted both theoretically and experimentally to create topographically rough surfaces with extremely high water-repellency and very low flow resistance.[1–3] By varying the surface chemistry using responsive polymer brushes,[4–7] surface roughness,[7–10] and external fields (*e.g.* electrowetting),[11,12] a number of groups have demonstrated dynamic tuning of surface wettability from superhydrophobic to hydrophilic. However, many questions remain as to how microscopic and nanoscopic roughness (surface chemistry, morphology, and geometry) contribute to the wettability and transition, and what is the range of liquid–air–substrate interaction along the grooves of a rough surface to achieve nonwettability, yet can be efficiently and reversibly switched to a wettable state. In addition, the issue of reversibility during operation and the feasibility of using a simple instrumental setup for switching could impose certain limitations on the realization of the work.

Previously, we have demonstrated reversibly tunable dry adhesion[13] on a rippled PDMS film by regulating the micro-scale surface roughness *via* mechanical strain. On the basis of the same tuning mechanism, here, we explore the dynamic switching of wetting behaviors[14] and flow resistance on the rippled PDMS bilayer film, as well as elucidation of wetting transitions between different states. While the water contact angle can be switched in real-time as a function of strain level, we and others[14] have observed that the water droplet tends to be pinned on the surface, suggesting a wettable contact described by the Wenzel's model.[15] In addition, the water contact angles on these micro-scale ripples are not high enough to guarantee superhydrophobicity, therefore, constraining the mobility of the droplets, and not achieving both tunable dry adhesion and self-cleaning as the gecko's foot manages to.[16] To promote surface wetting in Cassie's region,[17] which has a composite contact with water for low flow resistance, we integrate nanoparticles into the rippled system to generate dual-scale roughness. The dual roughness has been suggested to be critical to the observed superhydrophobicity in many aquatic plants,[18] which is confirmed and mimicked by various groups.[19–21] While other groups achieve tunable wetting by controlling surface chemistry[4–7] or nano-scale roughness,[7–10] here we present tunability adjusted by the microscopic roughness change resulting from mechanical force. In addition, the inclusion of superhydrophobicity within the tunable range of wetting behaviors directly implicates the switchability of flow resistance (*i.e.* droplet mobility *vs.* adhesion, or sliding and rolling), which potentially could lead to a broad range of engineering applications, such as microfluidic valves and mixers, anti-fouling materials, and manipulation of cell transport.

The fabrication procedure for the PDMS strip with a dual-structured surface is described as follows. First, the PDMS strip is clamped (Fig. 1a), mechanically stretched (Fig. 1b), and subjected to oxygen plasma treatment (Fig. 1c) to generate a stiff and thin oxidized siliceous layer on its top surface, which will be released later for the formation of the micro-scale ripple pattern.[22] Before releasing the stretched bilayer film, it is dip-coated with silica nanoparticles (Fig. 1d) for nano-scale roughness, which are subsequently hydrophobilized by (heptadecafluoro-1,1,2,2-tetrahydrodecyl)trichlorosilane (Fig. 1e). Finally, the dual-structured surface is obtained after releasing the initial strain (Fig. 1f) (see details in the Experimental section). When the sample is stretched back to the initial strain (Fig. 1g), the micro-scale rippled pattern is flattened,[13] therefore, only the nano-scale roughness remains. Formation of micro-scale ripple

[a]*Department of Mechanical Engineering, National Taiwan University, No. 1, Sec. 4, Roosevelt Road, Taipei, 10617, Taiwan*
[b]*Department of Materials Science and Engineering, University of Pennsylvania, 3231 Walnut Street, Philadelphia, PA 19104, USA. E-mail: shuyang@seas.upenn.edu; Fax: +1 (215) 573-2128; Tel: +1 (215) 898-9645*

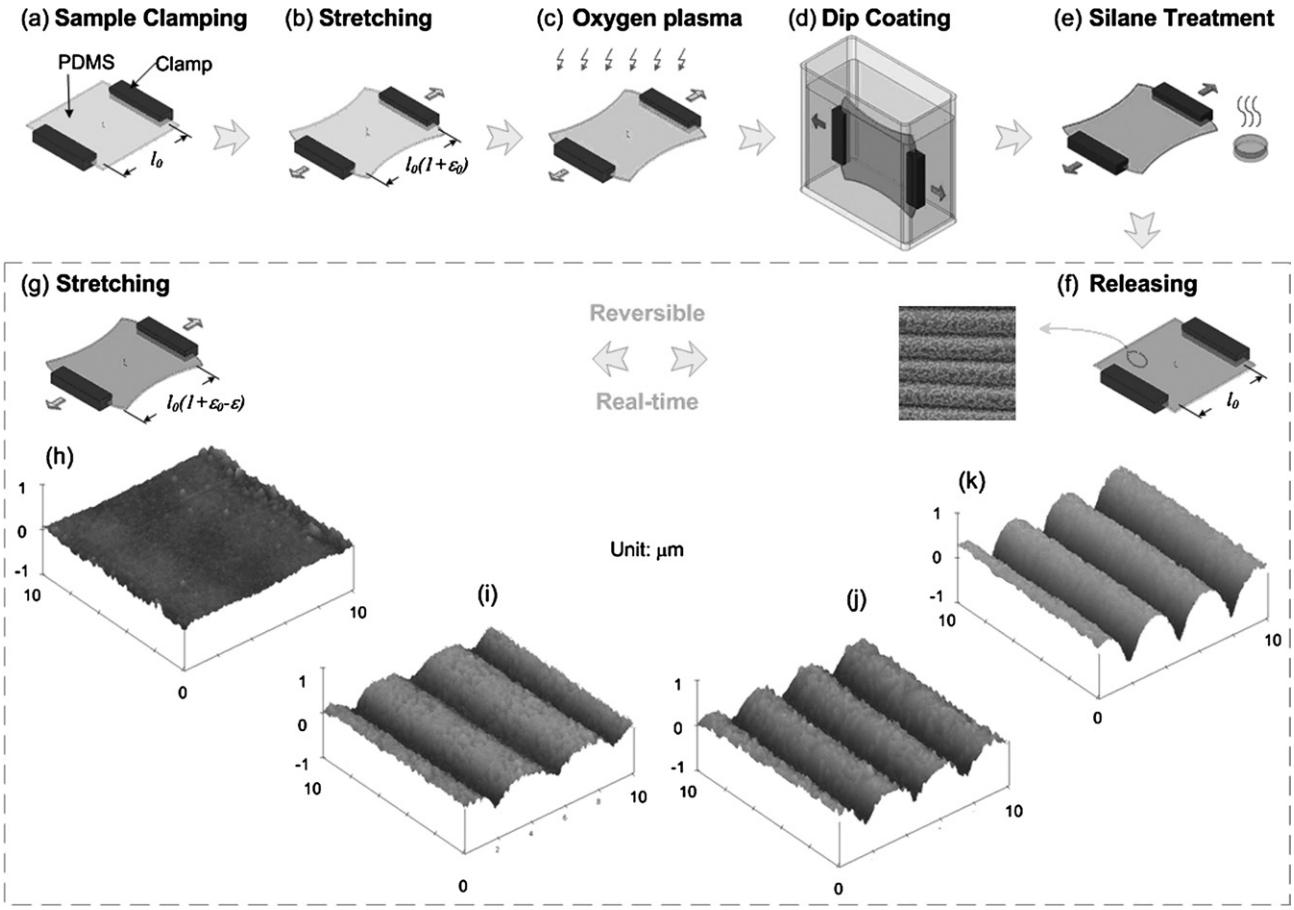

Fig. 1 A schematic illustration of the fabrication of a PDMS film with dual-scale roughness (a–f) and real-time, reversible tunability of its surface topography by mechanical strain (f–k). (a) Clamping a PDMS film. (b) Stretching the PDMS film to a designated initial strain value. (c) Oxygen plasma treatment. (d) Dip coating the stretched sample. (e) Silane treatment. (f) Releasing the stretch of the sample and spontaneous formation of micro-scale ripple patterns. (g) Stretching back the sample to the initial strain value. The ripple patterns disappear and only nano-scale roughness remains. (h–k) AFM images of the samples at different stretch conditions.

patterns on an elastomer has been demonstrated by various groups[23,24] for applications including phase grating,[25] anisotropic wetting,[14] and tunable adhesion.[13] However, there has been no attempt to combine this microstructure with nanoparticles to create a superhydrophobic surface, nor to control the wetting or flow resistance by regulating the topography of micro-scaled ripple patterns using a mechanical strain (Fig. 1f–1k).

Results and discussion

When the elastomeric PDMS film is subjected to an initial strain (ε_0) and oxygen plasma treatment, followed by releasing strain (ε) to a critical level (ε_c), a periodic one-dimensional sinusoidal ripple pattern is formed spontaneously:[26]

$$\varepsilon_c = \frac{1}{4}\left(\frac{3E_s(1-\nu_t^2)}{E_t(1-\nu_s^2)}\right)^{\frac{2}{3}}$$
$$\lambda_0 = \frac{\pi t}{\sqrt{\varepsilon_c}} \quad (1)$$

where E, ν, λ_0, A, and t are the Young's modulus, Poisson ratio, ripple wavelength, ripple amplitude, and thickness of the hard thin layer, respectively. The subscripts s and t denote the substrate and thin layer accordingly. The excess releasing strain beyond the critical strain, ε–ε_c contributes to the increase of the amplitude:[27,28]

$$A = t\sqrt{\frac{\varepsilon}{\varepsilon_c} - 1} \quad (2)$$

A dimensionless geometrical characteristic of the ripple pattern can be expressed by the ratio of the amplitude to the wavelength:

$$\frac{A}{\lambda_0} = \frac{\sqrt{\varepsilon - \varepsilon_c}}{\pi} \quad (3)$$

which is determined by the intrinsic material properties through ε_c.

When the wrinkled film is stretched back to ε_0, the surface returns to flat. Therefore, surface topography, including wavelength and amplitude, can be conveniently regulated by varying the applied strain level.[22] Previously we have demonstrated mechanically tunable dry adhesion for pick and release of a glass ball.[13] Here, we investigate the tunable wetting behavior and flow resistance modulated by the strain applied to the rippled surface with dual roughness. The wettability of the surface is usually

characterized by the water contact angle (CA), which is determined by both the surface energy (chemistry) and surface topography (physical roughness).

Wetting behavior of rippled PDMS surface

Two distinct models have been suggested by Wenzel[15] and Cassie[17] to explain the surface roughness effect on the contact angle. In Wenzel's model it is assumed that the liquid completely wets the grooves of the rough surface and roughness effectively increases the actual surface area. The apparent CA on a rough surface, θ_w, is a function of the Young's CA on a flat surface, θ:

$$\cos\theta_w = r\cos\theta \tag{4}$$

where r (>1) is the roughness factor, and defined as the actual surface area divided by the projected flat surface area in which the height variation is ignored.

For a very rough surface with a large Young's contact angle ($\theta > 90°$), the liquid does not fill the grooves on the rough surface. Instead, air is trapped below the liquid droplet and the surface can be considered as a composite surface of solid and air, which has a Cassie contact angle, θ_c:

$$\cos\theta_c = f_1\cos\theta - f_2 \tag{5}$$

where f_1 and f_2 are the fraction of solid–liquid and liquid–air contact areas, respectively.

A rough surface can have at least two possible apparent contact angles depending on the type of contact formed between the droplet and the substrate, θ_w and θ_c, corresponding to a wetted contact and a composite contact, respectively. The wetting behaviors of a sinusoidal rippled surface can also be described using both Wenzel's (Fig. 2a) and Cassie's models (Fig. 2b).[29] A transition from the Cassie region to the Wenzel region occurs if the following criteria is satisfied:[30]

$$\frac{A}{\lambda} < \frac{\tan\theta}{-2\pi} \tag{6}$$

which indicates that on a sinusoidal rippled surface, the wetting behavior is only determined by the dimensionless geometrical wave characteristics, A/λ, and Young's contact angle ($\theta > \pi/2$).

The static water CA of a flat PDMS film is measured as 105 ± 3°, which drops to 10° after oxygen plasma treatment but regains hydrophobicity, increasing to 50–60° after the PDMS film is relaxed in air for a few hours. Thus, in our experiments the oxidized PDMS was immediately treated with (heptadecafluoro-1,1,2,2-tetrahydrodecyl)trichlorosilane to raise the static CA to 112° ± 2°, which is used as the Young's contact angle, θ, for all calculations later in the text. According to eqn (6), to reach the Cassie state, A/λ should be larger than 0.39, whereas in our experiments the A/λ is typically in the range of 0.15–0.25 depending on the time of oxygen plasma treatment and amount of initial strain (up to 60%). The combination of eqn (3) and eqn (6) reveals that to achieve the Cassie contact angle of the ripples created here, the excess strain (ε–ε_c) has to be at least 153%, and that is $\varepsilon \approx 164\%$ for $\varepsilon_c \approx 11\%$ in our system.[13] However, the PDMS film breaks above $\varepsilon \approx 70\%$. Fig. 3 plots the trend of the wetting status derived from the combination of eqn (3) and eqn (6). It can be clearly seen that the Cassie scenario, in general, requires a high Young's contact angle, which is determined by surface chemistry, and high excess strain (ε–ε_c), where ε_c is determined by the intrinsic Young's moduli and Poisson ratios of bilayer materials [eqn (1)]. This plot also reveals that the trend is

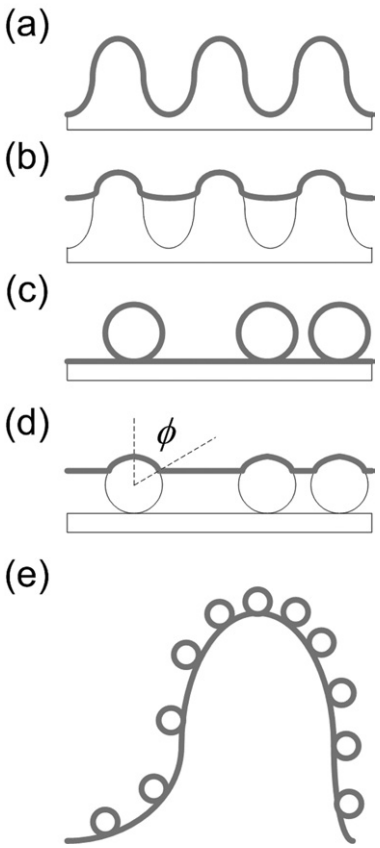

Fig. 2 Wetting behaviors of various surfaces. The thick gray line represents the wetting contact line. Wenzel's (a) and Cassie's (b) wettings on the micro-scale rippled surfaces. (c) Ideal Wenzel's (by ignoring the surface tension) and (d) simplified Cassie's wettings on the nano-scale nanoparticle surface. (e) Ideal Wenzel's wetting on the surface with dual-scale roughness. ϕ is the azimuthal angle, representing the wetting level on the sphere.

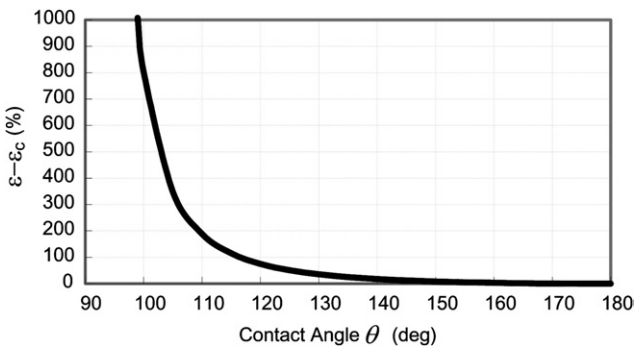

Fig. 3 Theoretical estimation of the wetting transition between Wenzel and Cassie regions of the rippled PDMS surface generated by internal buckling. ε–ε_c denotes the excess strain beyond the critical strain ε_c, and θ is the Young's contact angle of the flat surface.

highly sensitive to the Young's contact angle in the range of 100°–130°: a slightly increase in θ will dramatically reduce the required excess strain to be in the Cassie region. For example, when θ is increased from 112° to 120°, the excess strain is reduced from 153% to 75%, which becomes accessible when using a softer PDMS film by decreasing the ratio of crosslinker: PDMS precursor. We are currently investigating this possibility.

So far, all the contact angle analysis using eqn (1)–(3) and (6) are based on the assumption that surface geometry of ripples is sinusoidal. To validate this assumption, we performed a "contour length check" based on AFM images of the rippled surface. The normalized contour length of a sinusoidal wave can be expressed as

$$s = \frac{1}{\lambda}\int_0^{\lambda}\sqrt{1+\left\{\frac{\mathrm{d}}{\mathrm{d}x}\left[A\sin\left(\frac{2\pi x}{\lambda}\right)\right]\right\}^2}\,\mathrm{d}x \qquad (7)$$

Using experimentally measured λ and A from AFM, we obtain $s = 1.37 \pm 0.04$. Separately, experimental contour length can be directly measured by integrating the discrete points from the AFM image profile, yielding $s = 1.40 \pm 0.06$. The fact that the difference between two results is less than 5% validates our approximation of the actual geometry of ripples as sinusoids.

The normalized contour length s defined in eqn (7) is indeed equivalent to the roughness factor, r, defined in Wenzel's model, and approximately equivalent to the initial strain (ε_0) plus 1. During ripple fabrication the bulk PDMS is stretched from neutral length l_0 with an initial strain ε_0, thus, the neutral length of the thin oxide layer is $(1 + \varepsilon_0)l_0$. During the stretch releasing step (Fig. 1f), the thin layer is subjected to a compression force. Since the energy required to compress the thin hard layer is much larger than that to bend it,[13] the final contour length will remain nearly unchanged. Supporting this, the measured normalized contour length s from AFM minus 1 is 0.40 ± 0.06, which agrees perfectly well with the initial strain applied to the samples, $\varepsilon_0 = 40\%$. Given $\theta = 112°$ and $r = 1.4$, the apparent Wenzel contact angle of the rippled surface is calculated as 122°, which is consistent with our experimental observation, 124° ± 3° (Fig. 4a), a static CA viewed from the direction along with the ripple grooves ($\theta_{\|}$). More importantly, the agreement implies that the Wenzel contact angle of rippled surfaces generated by the bilayer buckling can be simply estimated according to the initial strain and Young's contact angle without the necessity of knowing the geometrical characteristics of ripples.

Both theoretical analysis and experimental study conclude that micro-scale rippled roughness is not sufficient to achieve the nonwettable Cassie state. This motivates us to explore surfaces with dual roughness by introducing nano-scale roughness onto the micro-rippled surface to mimic the dual roughness observed in natural surfaces,[18,21] which exhibit superhydrophobicity and low flow resistance. To generate nano-scale roughness, we dip-coated silica nanoparticles onto the PDMS film after stretching and plasma oxidation. The nanoparticle with diameter ~100 nm was selected for our experiments based on the observation by

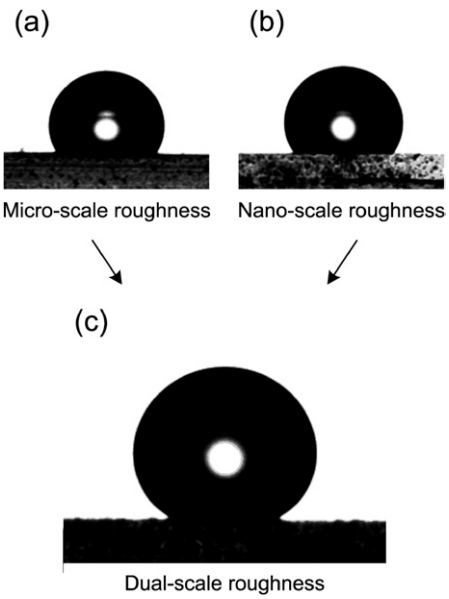

Fig. 4 Static contact angles of 6 μl water droplets on the various surface. (a) Ripple-patterns (micro-scale roughness). (b) A flat PDMS surface coated with silica nanoparticles (nano-scale roughness). (c) Dual-structure of silica nanoparticles coated on a rippled PDMS film (dual-scale roughness). (a) and (c) are viewed from the direction along the ripple grooves.

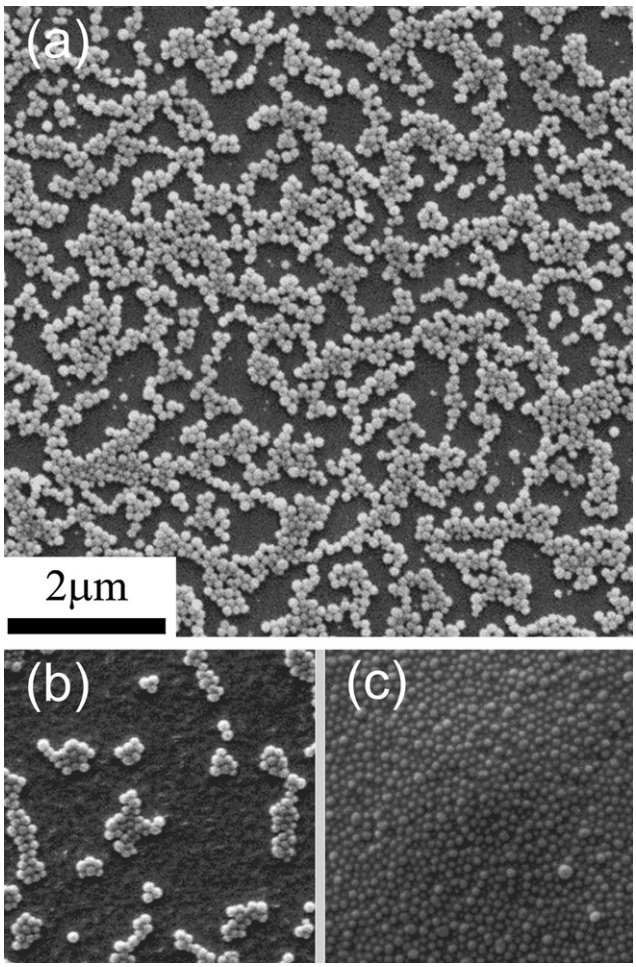

Fig. 5 SEM images of silica nanoparticles dip-coated at different concentrations onto the flat PDMS films. (a) $34 \pm 5 \times 10^{12}$ particles m^{-2}, (b) $9 \pm 3 \times 10^{12}$ particles m^{-2}, and (c) multi-layer full coverage.

other groups[19,20] using dual roughness to enhance the hydrophobicity. The particle concentration and withdrawing speed of the sample from the solvent bath was fine-tuned such that a monolayer of nanoparticles spread randomly on the surface (see Fig. 5a). A lower concentration of particles or slower withdrawing speed yielded low coverage of particles on the sample surface (see Fig. 5b). To the opposite, a higher concentration of nanoparticles or faster withdrawing speed yields a fragile multilayer coating (Fig. 5c), which can easily crack during the stretching/releasing steps to form micro-scale ripples.

We found that it was important to perform oxygen plasma treatment of the PDMS film prior to the dip-coating of nanoparticles. In the reverse order the nanoparticles coated on PDMS film will impede the O_2 gas diffusion during plasma treatment, resulting in the formation of irregular ripple patterns. Likewise, it was necessary to perform dip-coating before strain releasing; otherwise the nanoparticles would fill up the grooves of the ripples after the dip-coating. The order of silane treatment and strain releasing, however, was found not to be critical.

Wetting behavior of flat PDMS surface coated with silica nanoparticles

To study the wetting behaviors of the rippled surface with dual roughness, we first evaluated a flat PDMS film coated with silica nanoparticles only. A typical distribution and density of particles on the flat PDMS surface can be seen from Fig. 5a. The nanoparticle surface was subjected to the same oxygen plasma treatment as that in the ripple formation (see Fig. 1a, 1d, and 1e, followed by fluoroalkylsilane treatment, therefore, the underlying surface chemistry was identical to that of the later discussed dual-structures. We found that the AFM we used in the experiments, DI Dimension 3000, always underestimated the Wenzel roughness factor, r, due to its relatively low resolution, which could not generate sufficient data points to describe the curving surface contour of nanoparticles with diameter 70–100 nm (see Fig. 1). Thus, we estimated the roughness factor based on the "ideal" Wenzel's model with complete wetting depicted in Fig. 2c

$$r = 1 + N(4\pi R^2) \tag{8}$$

where N is the number density of particles ($34 \pm 5 \times 10^{12}$ particles m^{-2} estimated from Fig. 5a), and R is the radius of the particle in average (42.5 nm). Because the nanoparticles were randomly distributed on the flat surface in our system, to calculate the Cassie contact angle, we simplified the model by assuming that the composite wetting line holds at the same height and the liquid penetration between spheres can be ignored. Therefore, the fraction of solid–liquid contact is approximated as

$$f_1 = \frac{2\pi R^2(1-\cos\phi)N}{2\pi R^2(1-\cos\phi)N + (1-\pi(R\sin\phi)^2N)} \tag{9}$$

where the azimuthal angle ϕ represents the wetting level on the sphere depicted in Fig. 2d. The measured static contact angle of surfaces with nano-scale roughness is $128^\circ \pm 3^\circ$ (Fig. 4b), leading to roughness factor $r = 1.64$ according to eqn (4). From eqn (8), we estimate the Wenzel contact angle as 126°, in contrast to 143° when $\phi = 90^\circ$ (half wetting) using Cassie's model with f_1 defined in eqn (9), and 180° when $\phi = 0^\circ$. This suggests that the wetting behavior of the nanoparticle surface is also closer to the Wenzel's scenario, *i.e.* a wettable rough surface, as illustrated in Fig. 2c. The small discrepancy between the measured ($128^\circ \pm 3^\circ$) and predicted Wenzel contact angle (126°) could be due to air partially trapped in-between particles because the coating of particles may not be completely homogeneous on surface.

Wetting behaviors of rippled PDMS surface coated with nanoparticles

The surface with dual roughness became superhydrophobic with an apparent static water contact angle $150^\circ \pm 2^\circ$ (Fig. 4c). Since the length of surface contour does not change during ripple formation as discussed earlier, the Wenzel's roughness factor in this dual-structure can be estimated as $1.4 \times 1.64 = 2.296$ (Fig. 2e). At this high roughness ratio, we expect the water contact angle enters Cassie regime according to the study by Johnson and Dettre.[29] Supporting this is the measured contact angle hysteresis. As seen in Fig. 6, the flat sample has hysteresis 29.8°, which increases to 43.5° (viewed from the direction along with the ripple grooves) and 62.5° for the single-scale rough surfaces of micro-scale ripples and nanoparticle film, respectively. The contact angle hysteresis drops significantly to 11.3° on the surface with dual-scale roughness, which has energetically preferred composite configuration.[29]

Investigation of sliding angles on various surfaces

The observed superhydrophobicity together with low contact angle hysteresis of the surfaces with dual-scale roughness implies the reduction of flow resistance in comparison to the surface with either micro-scale or nano-scale only roughness. In the meantime, because the micro-scale ripple patterns can be reversibly controlled by the external strain, we anticipate that the flow resistance on surface with dual-scale roughness should also be

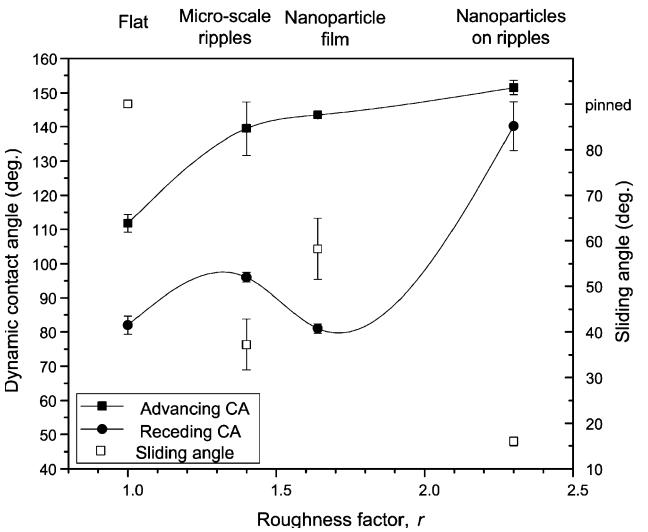

Fig. 6 Dynamic contact angles and sliding angles on various rough surfaces. For both rippled surfaces (micro-ripples and nanoparticles on micro-ripples), the contact angles were measured in the direction along with ripple grooves. Lines are used to guide the eyes, illustrating the change in contact angle hysteresis with roughness.

mechanically tunable. The flow resistance of the surface is quantified by the sliding angle, α, which is defined as the tilt angle when the liquid drop starts to move on a surface.[29] Theoretical modeling of the sliding angle on a flat surface was first addressed by Rosano[31] and Furmidge:[32]

$$\sin\alpha = \frac{1}{mg} B\gamma_{lv}(\cos\theta_r - \cos\theta_a) \quad (10)$$

where m is the mass of the liquid drop, g is the force due to gravity, γ_{lv} is the interfacial tension between liquid and vapor, and θ_a and θ_r are the advancing and receding contact angles, respectively. The shape of the drop is assumed rectangular, with $B = w$ as the width of the drop. Carre and Shanahan later modeled the droplet motion on an inclined plane by considering a droplet with a circular contour line,[33] and $B = \pi r_0/2$, which is commonly adopted to evaluate quantitatively the hydrophobicity of a flat polymer surface.[34] In these theoretical models the derivation of sliding angles is primarily based on the balance of force along sliding direction due to gravity of the droplet and the "restraining force" due to motion of the advancing/receding wetting lines, but no further discussion on the detailed interfacial motion (sliding or roll-off).[35] Here, the "sliding angle" is used based on the same definition in literature.

Fig. 7 shows the sliding angles of the surface with dual-scale roughness as a function of the external strains and associated Wenzel's roughness factor in comparison to several controlled surfaces. The volume of water drop is 10 μl for all experiments. For the pristine flat PDMS films, the droplet was pinned, and started to slide at ~80° only when its volume was increased to ~30 μl. For the ripple surfaces with only micro-scale roughness, the droplet began to move at $\alpha_{//} = 37° \pm 5.6°$ along the ripples grooves, and at $\alpha_{\perp} = 42° \pm 14°$ when perpendicular to the grooves. Because of the periodic sinusoid geometry of ripples, the contact line of droplet is anisotropic, that is the droplet will have no energy barrier to wet along the grooves compared to that perpendicular to grooves.[14] Such anisotropic wetting and sliding have been reported on surfaces with sinusoid geometry but larger

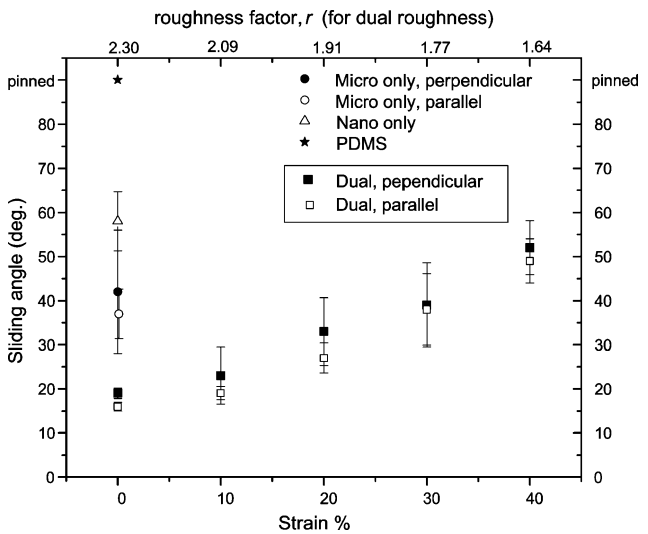

Fig. 7 Sliding angles *vs.* strain and roughness factor on surfaces with dual-scale roughness. Sliding angles from micro-ripples, nanoparticle film and flat PDMS film were collected for comparision.

wavelengths.[14,36,37] For the flat surface coated with nanoparticles, the droplet started to slide at $\alpha = 58° \pm 6.7°$. For the surfaces with dual-scale roughness (without external strain, full-sized ripples), the droplet started to slide at $\alpha_{//} = 16° \pm 1.0°$ along the ripple grooves and $\alpha_{\perp} = 19° \pm 1.2°$ perpendicular to the grooves. When the external strain was applied to the sample (Fig. 1k–h), the ripples gradually vanished, leaving only the nano-scale roughness remained on suface and the sliding angle increased back to $\alpha_{//} = 49° \pm 5.0°$ and $\alpha_{\perp} = 52° \pm 6.1°$. Overall, the sliding angle of dual-structured surface can be reversibly tuned approximately three times between the wrinkled dual structure and flat nanoparticle film, simply by varying the mechanical strain level applied to the PDMS film.

Previously, Song *et al.*[38] investigated the anisotropic sliding behavior of water droplets on flat micro-scale line-pattern surfaces from self-assembled monolayers (SAMs) of hydrophobic silanes. To quantify the effect of line direction on sliding behavior, they modified Carre's equation by introducing a correction for the fraction of solid–liquid contact. In comparison to their physically flat but chemically heterogeneous surfaces, our system with physical heterogeneity is much more complex to adapt eqn (10) for the prediction of sliding angles in parallel or perpendicular to the ripple grooves. To achieve a high contact angle and low contact angle hysteresis, it requires destabilizing the three-phase (solid–liquid–air) contact line.[39,40] In our systems, the meta-stable wetting depends on the jump of droplets on top of different nanoparticles on the same ridges of ripples or on adjacent ridges of ripples. This phenomenon is not included in the model of moving droplets on the flat surface, and we suspect this is also the main reason why the sliding angles are different along the direction of motion, where the ridges of ripples impose an energy barrier to confine the droplet spreading across it.

Experimentally we also observed that the sliding angles are slightly smaller if the drop moves along the grooves than perpendicular to them. Although quantitative understanding of the sliding behavior of our system is yet to be developed, the qualitative trend, low hysteresis and smaller contact area (high contact angle) yielding a low sliding angle agrees well with the prediction from eqn (10). Nevertheless, the sliding angle of our nanoparticles-on-ripples surface is somewhat larger than those reported from superhydrophobic surfaces with dual roughness.[20,41,42] It may be due to (1) the nature of the fluoroalkyltrichlorosilane treatment, which is very sensitive to the moisture, resulting in a large chemical heterogeneity and hysteresis, and (2) both the topography and chemical heterogeneity of the surface[29] triggered by the stretching/releasing cycles, where pure PDMS, oxidized PDMS, silica, and fluoroalkylsilane co-exist on the surface. To address this, we are currently investigating fine control of uniformity of the nanoparticle distribution as well as, for example, using alkyldimethylchlorosilanes,[43] which have been reported with low water contact angle hysteresis, ~10°.

Conclusion

We construct a new elastomeric material consisting dual-scale roughness, which exhibits mechanically-tunable wetting and sliding behaviors. The micro-scale roughness is created from internal buckling of a PDMS elastomer bilayer film, whose surface

roughness can be reversibly regulated by applying mechanical strain. The nano-scale roughness is generated by conformal coating of silica nanoparticles on the rippled PDMS surface, which promotes the wetting transition from a Wenzel regime (on both micro-rippled PDMS and nanoparticle film) into a Cassie regime (on the dual-rough surface). The sliding angle of the dual-scale rough surface is reduced at least three times in comparison to the surfaces with single-scale roughness, which can be mechanically tuned simply by varying the stretch strain level. The anisotropic sliding behavior due to heterogeneous rough structure of surfaces is also observed. We are currently investigating the anisotropy dependent on the ripple wavelength/amplitude and surface chemistry. We believe the study presented here will offer new insight into the design of rough surfaces for tunable wetting and flow resistance, which will be valuable for the advancement of many existing technologies, including micro- and nano- fluidic applications, electronics and optoelectronics, as well as for driving new paradigms in biotechnology and soft robotics.

Experimental

PDMS sheet preparation

PDMS precursor (RTV615 from GE Silicones) was mixed with curing agent (10 : 1 wt/wt) and sandwiched between two $12'' \times 3''$ borosilicate flat-plate glasses using 0.5 mm-height shims as spacers. They were held together by 10 large $2''$ binder clips and cured at 65 °C for 4 h in a forced-air convection oven. After curing, the PDMS sheet (thickness of 0.5 ± 0.02 mm) was cut into 40 mm $\times$ 15 mm strips for experiment.

Micro-scale ripple pattern generation

The ripple patterns were generated in PDMS strip following the method reported earlier.[22] In brief, the PDMS strip was clamped (Fig. 1a) by two $3/4''$ small binder clips with nominal length (l_0) of 30 mm and mounted on the custom-made stretching jig composed of one large acrylic base and two sliders, whose positions could be adjusted continuously in real-time by two 30 mm-long M4 wing screws with pitch 0.7 mm. The PDMS strip was then stretched to the designated initial strain level ($\varepsilon_0 = 40\%$, Fig. 1b), followed by exposure to oxygen plasma (Technics, model PE11-A) with power setting at 100 watts, time duration of 180 s, and pressure at 550 mTorr (Fig. 1c).

Nano-scale roughness generation

The nano-scale roughness was achieved by dip-coating (Fig. 1d) the stretched samples in the solution of silica colloidal particles with diameter 70–100 nm (ORGANOSILICASOL™ IPA-ST-ZL, Nissan Chemical). The as-received silica particles solution (30 wt% in isopropanol) was diluted to 5% in ethanol for better dip-coating characteristics. The sample was immersed in ethanol for 5 s, followed by withdrawing into the air at a speed of 5 mm min^{-1}. After the dip-coating, the stretched sample was subjected to another light oxygen plasma treatment (30 W, 1 min) to enhance the bonding between silica nanoparticles and the rippled PDMS film, as well as to generate hydroxyl groups for vapor deposition of (heptadecafluoro-1,1,2,2-tetrahydrodecyl)trichlorosilane (SIH5841.0, from Gelest) (Fig. 1e). A couple of drops of trichlorosilane were placed on a petri dish in a low-pressure desiccator together with the sample for overnight. A surface with dual-roughness structure was formed spontaneously upon release of the initial strain, and reached the final shape when the external force was completely removed (Fig. 1f).

Sample characterization

Scanning electron microscopy (SEM) images were taken with a FEI Strata DB235 Focused Ion Beam in high vacuum mode with an acceleration voltage of 5 kV. Surface topography was imaged by a DI Dimension 3000 Atomic Force Microscope (AFM) in tapping mode. The contact angles were measured using Ramé-Hart Goniometer Model 200 with DROPimage Standard Software by averaging over 5 fresh points. In our current setup because the two clamps used for control of the mechanical strain (see Fig. 1g) interfered with the camera to capture the contact angles in the direction perpendicular to the direction of ripple grooves, the contact angles reported here were from the direction viewed along the ripple grooves.

Acknowledgements

This work has been supported in part by National Science Council (NSC), Taiwan, NSC 97-2218-E-002-022, National Science Foundation (NSF) CAREER award # DMR-0548070, and Nanotechnology Institute Proof-of-Concept (PoC) Fund. We also thank Krishnacharya Khare for critical reading of the manuscript.

References

1 D. Oner and T. J. McCarthy, *Langmuir*, 2000, **16**, 7777–7782.
2 J. Bico, C. Tordeux and D. Quéré, *Europhys. Lett.*, 2001, **55**, 214–220.
3 C. Cottin-Bizonne, J.-l. Barrat, L. Bocquet and E. Charlaix, *Nat. Mater.*, 2003, **2**, 237–240.
4 S. Minko, M. Muller, M. Motornov, M. Nitschke, K. Grundke and M. Stamm, *J. Am. Chem. Soc.*, 2003, **125**, 3896–3900.
5 T. L. Sun, G. J. Wang, L. Feng, B. Q. Liu, Y. M. Ma, L. Jiang and D. B. Zhu, *Angew. Chem., Int. Ed.*, 2004, **43**, 357–360.
6 R. Rosario, D. Gust, A. A. Garcia, M. Hayes, J. L. Taraci, T. Clement, J. W. Dailey and S. T. Picraux, *J. Phys. Chem. B*, 2004, **108**, 12640–12642.
7 N. Zhao, X. Y. Zhang, X. L. Zhang and J. Xu, *ChemPhysChem*, 2007, **8**, 1108–1114.
8 G. P. Li, T. Chen, B. Yan, Y. Ma, Z. Zhang, T. Yu, Z. X. Shen, H. Y. Chen and T. Wu, *Appl. Phys. Lett.*, 2008, 92.
9 Y. Yao, X. Dong, S. Hong, H. Ge and C. C. Han, *Macromol. Rapid Commun.*, 2006, **27**, 1627–1631.
10 K. Tsougeni, A. Tserepi, G. Boulousis, V. Constantoudis and E. Gogolides, *Japanese J. Appl. Phys., Part 1: Regular Papers Brief Communications and Review Papers*, 2007, **46**, 744–750.
11 T. N. Krupenkin, J. A. Taylor, T. M. Schneider and S. Yang, *Langmuir*, 2004, **20**, 3824–3827.
12 K. Khare, S. Herminghaus, J. C. Baret, B. M. Law, M. Brinkmann and R. Seemann, *Langmuir*, 2007, **23**, 12997–13006.
13 P. Lin, S. Vajpayee, A. Jagota, C. Hui and S. Yang, *Soft Matter*, 2008.
14 J. Y. Chung, J. P. Youngblood and C. M. Stafford, *Soft Matter*, 2007, **3**, 1163–1169.
15 R. N. Wenzel, *Ind. Eng. Chem.*, 1936, **28**, 988–994.
16 W. R. Hansen and K. Autumn, *Proc. Nat. Acad. Sci. U. S. A.*, 2005, **102**, 385–389.
17 A. B. D. Cassie and S. Baxter, *Trans. Faraday Soc.*, 1944, **40**, 0546–0550.
18 W. Barthlott and C. Neinhuis, *Planta*, 1997, **202**, 1–8.
19 N. A. Patankar, *Langmuir*, 2004, **20**, 8209–8213.

20 W. Ming, D. Wu, R. van Benthem and G. de With, *Nano Lett.*, 2005, **5**, 2298–2301.
21 L. C. Gao and T. J. McCarthy, *Langmuir*, 2006, **22**, 2966–2967.
22 P. Lin and S. Yang, *Appl. Phys. Lett.*, 2007, **90**, 241903.
23 N. Bowden, S. Brittain, A. G. Evans, J. W. Hutchinson and G. M. Whitesides, *Nature*, 1998, **393**, 146–149.
24 E. P. Chan and A. J. Crosby, *Soft Matter*, 2006, **2**, 324–328.
25 C. Harrison, C. M. Stafford, W. H. Zhang and A. Karim, *Appl. Phys. Lett.*, 2004, **85**, 4016–4018.
26 H. G. Allen, *Analysis and Design of Structural Sandwich Panels*, Pergamon Press, 1st edn, 1969.
27 X. Chen and J. W. Hutchinson, *J. Appl. Mech. Trans. ASME*, 2004, **71**, 597–603.
28 Z. Y. Huang, W. Hong and Z. Suo, *J. Mech. Phys. Solids*, 2005, **53**, 2101–2118.
29 R. E. Johnson and R. H. Dettre, *Surf. Colloid Sci.*, 1969, **2**, 85–153.
30 G. Carbone and L. Mangialardi, *Eur. Phys. J. E*, 2005, **16**, 67–76.
31 J. L. Rosano, *Mem. Serv. Chim. Etat.*, 1951, 36.
32 C. G. Furmidge, *J. Colloid Sci.*, 1962, **17**, 309.
33 A. Carre and M. E. R. Shanahan, *J. Adhes.*, 1995, **49**, 177–185.
34 N. Yoshida, Y. Abe, H. Shigeta, A. Nakajima, H. Ohsaki, K. Hashimoto and T. Watanabe, *J. Am. Chem. Soc.*, 2006, **128**, 743–747.
35 M. Nosonovsky, *J. Chem. Phys.*, 2007, 126.
36 Z. Yoshimitsu, A. Nakajima, T. Watanabe and K. Hashimoto, *Langmuir*, 2002, **18**, 5818–5822.
37 F. X. Zhang and H. Y. Low, *Langmuir*, 2007, **23**, 7793–7798.
38 J. H. Song, M. Sakai, N. Yoshida, S. Suzuki, Y. Kameshima and A. Nakajima, *Surf. Sci.*, 2006, **600**, 2711–2717.
39 W. Chen, A. Y. Fadeev, M. C. Hsieh, D. Oner, J. Youngblood and T. J. McCarthy, *Langmuir*, 1999, **15**, 3395–3399.
40 J. P. Youngblood and T. J. McCarthy, *Macromolecules*, 1999, **32**, 6800–6806.
41 Y. Li, C. C. Li, S. O. Cho, G. T. Duan and W. P. Cai, *Langmuir*, 2007, **23**, 9802–9807.
42 L. B. Zhang, H. Chen, J. Q. Sun and J. C. Shen, *Chem. Mater.*, 2007, **19**, 948–953.
43 A. Y. Fadeev and T. J. McCarthy, *Langmuir*, 1999, **15**, 3759–3766.

